JOURNAL OF MATERIALS RESEARCH AND TECHNOLOGY 2023;26:1785–1797

Available online at www.sciencedirect.com

jmr&t Journal of Materials Research and Technology

journal homepage: www.elsevier.com/locate/jmrt

Partially reduced graphene oxide produced by glucose in alkaline conditions using probe sonication: the role of the base in reduction

Jean Valdir Uchôa Teixeira [a], *Gabriel Junior Cavalcante Pimentel* [b], *Adriana Alencar Santos* [a], *Leonardo Francisco Gonçalves Dias* [a], *Valmor Roberto Mastelaro* [c], *Paulo Noronha Lisboa-Filho* [d,*]

[a] UNESP - São Paulo State University, Department of Physics, School of Sciences, Materials Science and Technology Program, 17033-360, Bauru, SP, Brazil
[b] UNESP - São Paulo State University, Department of Chemistry, School of Sciences, 17033-360, Bauru, SP, Brazil
[c] USP - Physics Institute of São Carlos, University of São Paulo, 13560-970, São Carlos, SP, Brazil
[d] UNESP - São Paulo State University, School of Science, Department of Physics, 17033-360, Bauru, SP, Brazil

ARTICLE INFO

Article history:
Received 6 May 2023
Accepted 25 July 2023
Available online 29 July 2023

Keywords:
Reduced graphene oxide
Chemical reduction
Glucose
Sono-assisted reduction

ABSTRACT

The use of mild reagents in the synthesis of reduced graphene oxide (RGO) is an advantageous method to produce materials partially reduced without the use of hazardous chemicals, such as the hydrazine route, which is a standard method to promote the chemical reduction of graphene oxide. This paper presents the sono-assisted route to produce partially RGO particles using glucose as a mild reducing agent in alkali media, mediated by sodium and potassium hydroxide. The results demonstrated the direct influence of base on the final properties of RGO, with differences in the thermal stability, bandgap, impedance, and C/O rate. With a possible anchoring of glucose-derivated molecules on sheet surface, this study indicates a way to control the particle surface properties according to the base chosen during the sono-assisted reduction method.

1. Introduction

Graphene is a bidimensional material composed of one layer of carbon in sp^2 hybridized, forming hexagonal honeycomb-like structures [1,2]. In a large number of stacked layers, it is called graphite. This large quantity of graphene layers can be used to obtain the graphene-based nanomaterial using methods such as the Scotch method of physical exfoliation [3,4], or chemical oxidation [5,6]. Furthermore, posterior reduction can be used to obtain a material with partial restoration on a hexagonal carbon honeycomb, but with residual interactions, which gives it interesting properties according to reduction conditions [7].

Different approaches are available to promoting graphene oxide reduction, with the first chemical reductions proceeding with hydrazine monohydrate, a potent reduction agent [8]. However, a drawback of this process is the toxicity of the compound to the environment and human health [8,9]. Therefore, the pursuit of new, safe, and eco-friendly

* Corresponding author.
E-mail address: paulo.lisboa@unesp.br (P.N. Lisboa-Filho).
https://doi.org/10.1016/j.jmrt.2023.07.211

alternatives called green chemical reduction methods are important [10–14].

The use of sugars as mild reducers to produce partially reduced graphene oxide (RGO) has been investigated. Stable RGO solutions have been applied in the biomedical field, as support in cancer therapy [15–18], electrocatalysis [7,19], conductive ink [20–22], and fabrication of composites based on RGO [23,24], mainly due to the interaction between graphene sheets and the open-chain oxidized glucose molecules [10]. Furthermore, this green approach based on glucose oxidation can produce materials with different degrees of carbon restoration, with consequent variations in C–C\C–O and in the bandgap of the material, which are important characteristics for further applications.

We present a synthesis of RGO using glucose in alkaline conditions, employing NaOH and KOH as the base to promote graphene oxide reduction, unlike previous reports that promoted pH adjustments with an ammonia solution [20,25]. The process, assisted by probe sonication, achieved different levels of oxidation according to the base chosen, with impacts in the electronic transport confirmed by bandgap and impedance parameters, and on the content of hydroxyl attached, due to the consequent interactions with glucose-oxidized molecules.

2. Materials and methods

2.1. Materials

Graphite powder (CAS: 7782-42-5; particle size <20 μm), potassium permanganate (CAS: 7722-64-7; $KMnO_4$), and D-(+)-Glucose (CAS: 50-99-7, $C_6H_{12}O_6$) were purchased from Sigma Aldrich. Sulfuric acid (CAS: 7664-93-9; H_2SO_4) and potassium hydroxide (CAS: 1310-58-3; KOH) were obtained from *Química Moderna*. Sodium hydroxide (CAS: 1310-73-2; NaOH) was purchased from Synth. All the chemicals were used without any further purification.

2.2. Synthesis of graphene oxide

A modified Hummers' method was applied for the exfoliation and oxidation of graphite. First, 3 g of graphite powder was loaded into a beaker, and 100 mL of ultrapure water was added. The product was sonicated by an ultrasonic tip for 10 min using 40% of total power at 20 kHz ±50 Hz. Later, the material was centrifuged at 8000 RPM in water: alcohol solution (4:1 v/v) and dried at 60 °C overnight.

The dried material (3 g) was dispersed in 90 mL of sulfuric acid and stirred for 20 min. Then, 7.5 g of potassium permanganate was slowly added in the ice bath. After this, the solution was stirred for 30 min. The solution was placed at ambient temperature (around 30 °C) and stirred for 10 min, followed by bath sonication for another 10 min. Aliquots of 50 μL were taken every 3 cycles of stirring and sonication to investigate the oxidation process with UV spectroscopy. The process was finished after 15 cycles. After that, 100 mL of pure water was added to the solution in the ice bath, and the final solution was sonicated in an ultrasound bath for 120 min, with posterior decantation overnight and centrifugation in ultrapure water at 8000 RPM, until the solution reached pH 5. Last, the precipitated material was dried at 60 °C overnight.

2.3. Reduction of graphene oxide

The graphene oxide (GO) reduction was performed by chemical reduction using glucose in alkaline conditions with slight modifications. First, 50 mg of GO was loaded into a beaker, and 100 mL of 0.1 M glucose aqueous solution was added. The mixture was sonicated by ultrasonic tip for 20 min using 40% of total power at 20 kHz ±50 Hz. Then, 150 μL of 1 M NaOH or KOH solution was added every 10 min for 50 min while the beaker was under sonication. Then the solution remained for another 10 min without the addition of base. Visible spectroscopy (UV–Vis) absorbance measurements were performed every 10 min after sonication to monitor the graphene oxide reduction process. Finally, the material was centrifuged at 8000 RPM for 10 min, and the precipitate was washed twice with ethanol and a third with ultrapure water, with subsequent drying in a desiccator for 48 h.

2.4. UV–Visible spectroscopy (UV–Vis)

The UV–Vis absorption spectra were recorded using a UV–Vis spectrophotometer (UV-1800 Shimadzu) in the range of 600–200 nm. For the sample, 50 μL of the mixture was diluted in 950 μL of deionized water, using 1 mL of deionized water as a blank. Then, the material powder was diluted in deionized water (0.5 mg/mL) for bandgap measurements and sonicated for 30 s. All the measurements were done with a pair of quartz cuvettes.

2.5. Characterization

Infrared spectroscopy analysis was performed in the attenuated total reflection (ATR-FTIR) (Vertex 70, Bruker) with a range from 400 cm^{-1} to 4000 cm^{-1} in transmittance mode, with 32 measurements per sample. The thermogravimetric analysis was performed at STA 449 F3 (NETZSCH), with 5 mg for each sample, heating of 10 °C/min, and air atmosphere (50 mL/min), at 30–700 °C. The X-ray diffraction (XRD) was performed varying from 5° to 80°, with a step of 0.02 and a copper X-ray source. Scanning Electron Microscopy (SEM) was performed using FEG-MEV (JEOL, 7500F) microscopy. Electrochemical impedance spectroscopy (EIS) was applied in PBS at pH 7.4 as electrolyte. EIS was recorded at frequencies ranging from 10^5 to 0.1 Hz, using 10 mV varying the frequencies, with the acquisition of 10 points per decade. The EIS data were analyzed with the Metrohm Autolab potentiostat NOVA software (version 2.1). The chemical composition of prepared materials was accessed using X-ray photoelectron spectroscopy (XPS, Scienta Omicron ESCA), with an EA125, Xm1000 monochromator, and Al Kα (1486.7 eV) X-ray source. Survey spectra were collected using a pass energy of 50 eV and an energy step of 0.5 eV. High-resolution spectra were obtained with a pass energy of 50 eV and an energy step of 0.05 eV. The XPS spectra were analyzed using CasaXPS software; the binding energy was corrected using the C1s signal of aliphatic hydrocarbon species at 285.0 eV. Atomic surface

concentration was evaluated based on Scofield's relative sensitivity factor (RSF).

3. Results and discussion

The research findings are presented to demonstrate the modifications in graphene-based materials after each synthesis step, followed by the obtained RGO characterization.

3.1. Synthesis

3.1.1. Oxidation of graphite

The oxidation evolution can be observed in Fig. 1. The UV–Vis spectra present step 0- after adding $KMnO_4$ and stirring for 20 min, up to step 15, corresponding to the successive ultrasound bath and stir process.

The oxidation response was verified after step 9, with a broad absorbance peak of 265 nm and a shoulder on 285 nm, which was attributed to the transitions $\pi \rightarrow \pi^*$ and $n \rightarrow \pi^*$. However, the broad aspect was due to the presence of flakes with different degrees of oxidation on the solution. After step 15, an increase in absorption at 265 nm was observed, possibly due to the exfoliation and oxidation process leading to the exfoliation of graphite flakes and subsequent oxidation. Therefore, 265 nm peak was adopted as a standard for further reduction and characterization.

3.1.2. Reduction of graphene oxide (GO)

The reaction was performed in different conditions and monitored by periodic UV/Visible analysis. In this work, we considered the product reduced when the maximum absorbance peak concerning the transitions $\pi \rightarrow \pi^*$ reaches wavelengths greater than or equal to 260 nm.

Fig. 2a and b presents the different behaviors found by adding the total volume (750 μL) or small portions (150 μL) of alkali during the process, which are labeled as triangles (O termination) and square (S termination) dots, respectively. The latter follows the procedure previously related, and for both cases, the GO was dispersed in a glucose aqueous solution for 20 min. With the total volume of hydroxide added, the bathochromic shift of the maximum peak at around 230 nm started with the addition of the alkali, with the reduced product being obtained after 20 and 30 min of sonication with the base of KOH and NaOH, respectively.

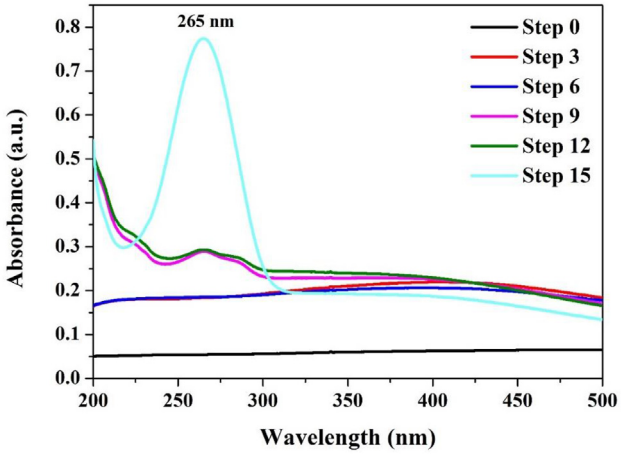

Fig. 1 – UV–Vis spectra recorded during the oxidation process with each step corresponding to the successive 10 min ultrasound bath followed by 10 min of stirring.

Furthermore, the absorbance of this peak increased in the first 40 min of sonication using NaOH, and 50 min using KOH, decreasing its value after this period, possibly due to the degradation of glucose derivate capping agent [9]Reducing the hydrophilicity compound caused agglomeration of partially RGO with the formation of a black precipitated [26].

However, adding the same volume in small portions during the process led to the maximum shift beginning after 20 min, with a reduced product obtained after 50 min. In this case, the maximum absorbance value increased at the beginning and after 40 min, especially for NaRGO. This increase, for both bases, occurs even with a slight variation in the maximum wavelength. With NaOH, the absorbance presents a value greater than the total volume added. After 60 min of sonication, the dispersion was unstable and there was an agglomeration of the formed product, decreasing the absorbance using both bases. Due to these behaviors, NaRGO/S and KRGO/S (with S referring to the adding of the total volume (750 μL) in fractions) were selected as products of interest, and then renamed NaRGO and KRGO.

To emphasize the synergy effect of the reducing agents, other reaction conditions were varied as presented in Fig. 2c. The plots illustrate that the process performed with only alkali or glucose as a reducing agent does not produce RGO, with a wavelength of the maximum remaining constant at around 230 nm. During the preparation of partially reduced graphene oxide from graphene using glucose under alkaline conditions involving probe-sonication, it is possible to produce free radicals during acoustic cavitation, which in turn act as reducing agents. However, it is important to emphasize that, considering the low power applied to the system in this case, there is a negligible effect of reactive oxygen species formation during water sonolysis, which is a process where reduction of graphene oxide could also occur without the addition of a base [27,28].

The bathochromic shift only occurs with GO dispersion in the presence of glucose and NaOH or KOH, reaching values at around 270 nm and resulting in a reduced product. This finding can be due to the oxidation of the open-chain molecules of gluconic acid, which interact with oxygenated groups on graphene, serving as a catalyst in the basic media to the graphene deoxygenation [8,10].

3.2. Characterization

3.2.1. UV–Vis spectroscopy

The UV–Vis spectra of centrifuged and redispersed RGO and GO samples were recorded to evaluate the optical properties of the obtained material, as presented in Fig. 3. Both products (KRGO and NaRGO) present similar behavior. For GO, a typical absorption peak at 233 nm appears, which is attributed to the $\pi \rightarrow \pi^*$ transition of the aromatic C=C bonds. In addition, the broad shoulder peak, at around 300 nm, is attributed to $n \rightarrow \pi^*$ transitions of the carbonyl groups [29]. The latter occurs in

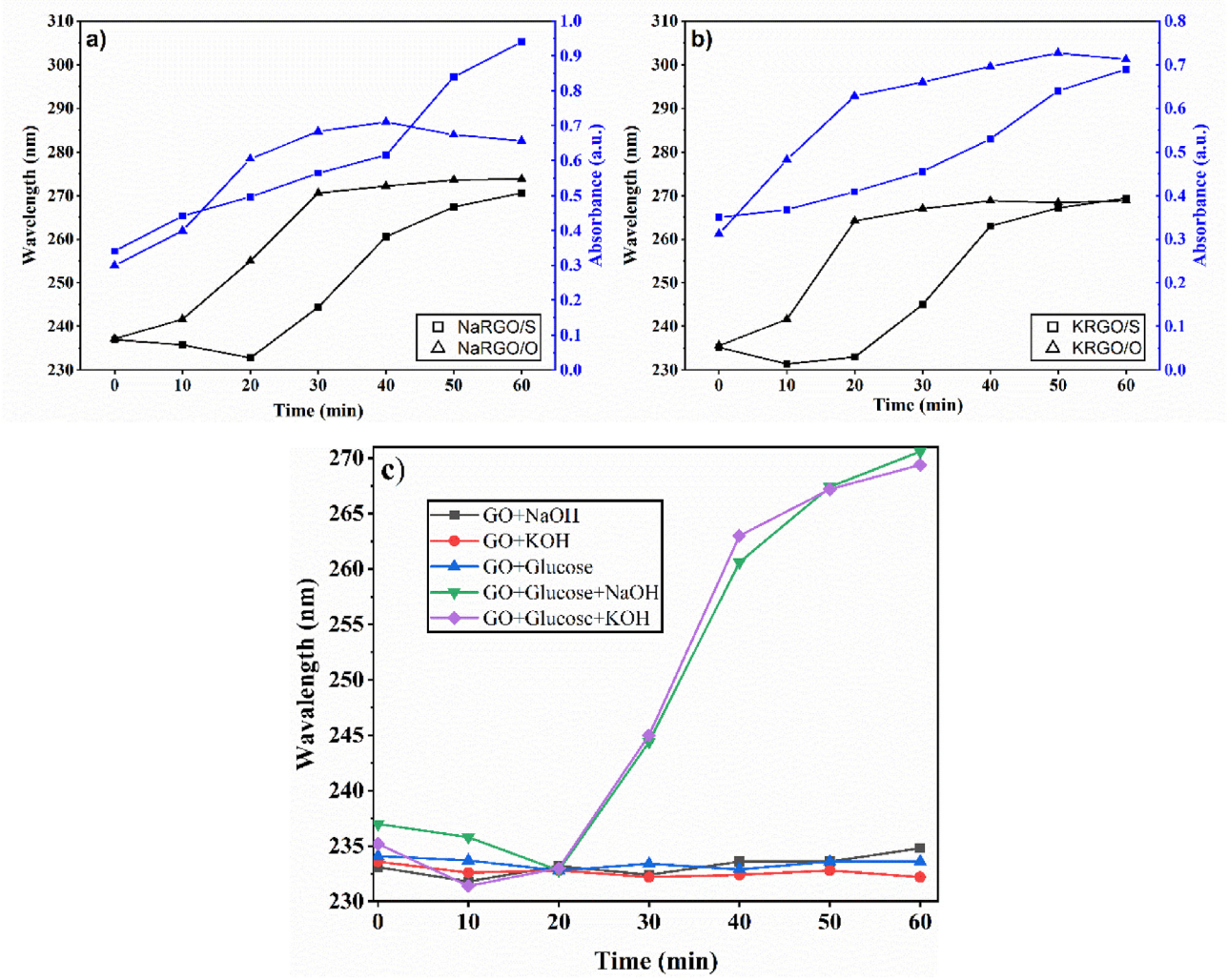

Fig. 2 – UV–Vis spectral analysis of maximum wavelength and intensity during the reduction of NaRGO (a), KRGO (b), and the compositions of the different solutions for 60 min (c). samples differing by adding the total volume (750 μL) or small portions (150 μL) of alkali during the process, which are labeled as triangles (O termination) and square (S termination) dots, respectively.

fewer numbers than the $\pi \rightarrow \pi^*$ transitions, which explains the lower absorbance peak.

After the process, the absorption peak at 233 nm red-shifted to 270 nm and 273 nm, for NaRGO and KRGO, respectively. This suggests that the aromatic carbon sp^2 structure, previously affected by the oxidation process, was partially restored. Moreover, the broad shoulder peak disappeared after the reduction, indicating the removal of oxygen from the lattice of graphene oxide. These findings are consistent with the visual change in color of graphene, from yellowish-brown to black [30].

From the UV spectra, Tauc plot extrapolation was performed to obtain the optical bandgap values presented in Table 1. When the conjugated structure is restored, the p orbitals combine again and the difference of energy between the orbitals HOMO and LUMO is decreased [29]. This event can be associated with variations in the bandgap energy in the material, with values from the theoretical 0 eV in graphene single sheet [31,32] up to 3.67 eV in the oxidized graphene. These phenomena occur due to the presence of oxygen bonds, reducing the free-moving distance traveled by electron on the carbon rings, consequently increasing the bandgap.

When the reduction was performed, a partial restoration of carbon bonding occurred, which decreased the distance between the valence and conduction band. This in turn reduced the bandgap to 2.64 eV in NaRGO and 2.48 eV in KRGO, with this discrepancy attributed to deoxygenation of epoxy and hydroxyl bonds on the sheets, allowing a partial restoration of free-moving electron.

3.2.2. *Fourier transform infrared spectroscopy (FTIR)*

To understand the variations in the oxygen content groups bonded to carbon sheets after the chemical reduction process, ATR-FTIR was performed, and the results presented in Fig. 4. Infrared spectroscopic confirmed the presence of the expected chemical functionalities on graphene oxide and its decrease in the reduced products, especially in the regions of 1000 cm^{-1}, 1200 cm^{-1}, 1600 cm^{-1}, and 3000 cm^{-1} up to 3600 cm^{-1}.

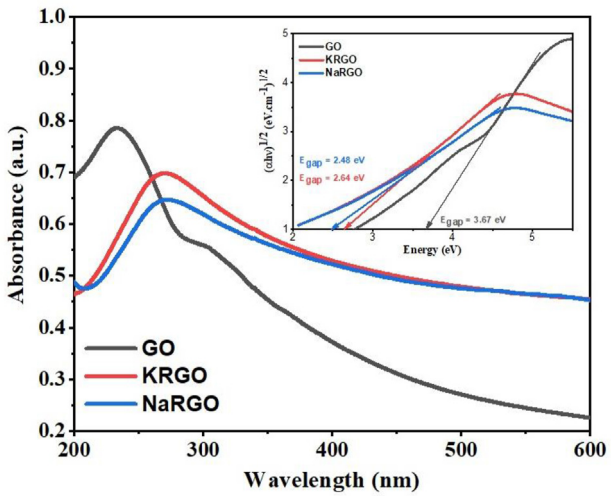

Fig. 3 – UV spectra of synthesized GO, GO reduced with NaOH (NaRGO), and KOH (KRGO) with their respective bandgaps in the onset rectangle.

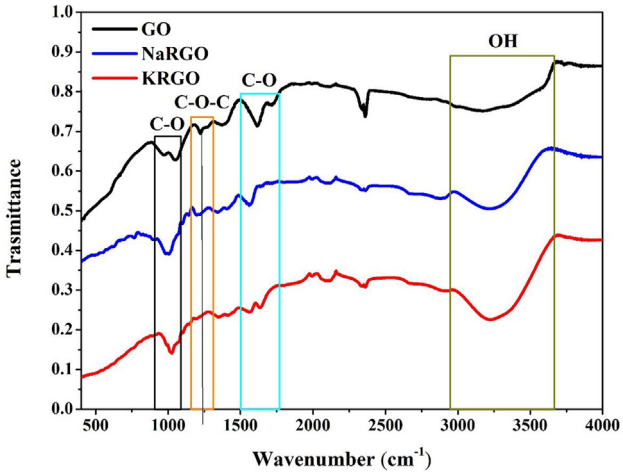

Fig. 4 – ATR-FTIR spectra of graphene derivated samples, black line = graphene oxide, blue line = reduced graphene oxide (RGO) reduced with NaOH labeled (NaRGO), and redline = RGO reduced with KOH (KRGO). The colored rectangles correspond to the variation in C–O, C–O–C, and –OH bonds.

The region of about 1000 cm^{-1}, with the presence of two identified bands in 960.4 cm^{-1} and 1056.9 cm^{-1} on graphene oxide, corresponds to the vibrations of C–H and C–OH stretching, with the conversion of a single band on the reduced product in 1004.8 cm^{-1} in NaRGO. In KRGO, 1026.0 cm^{-1} corresponds to hydrogen bend vibration on the carbon ring and disappearance of hydroxyl attached correspondent bond.

Following the increase in wavelength, a band at 1224.7 cm^{-1} corresponds to the vibration of oxygen attached to the carbon ring in GO derivate from epoxy groups. Its displacement to 1197.7 cm^{-1} can be attributed to C–O stretching in NaRGO and is absent in KRGO. This variation can be attributed to the reduction of oxygen substituting carbon density in the reduced product, with a break in the chains and the formation of oxygenated groups in edges of graphene sheets.

In the sequence, the spectra show a representative band at 1616.2 cm^{-1} from the presence of unoxidized domains at carbon layers on GO, following previous reports with GO obtained from Hummer's method and its variations [33,34]. In addition, the band at 1716.5 cm^{-1} corresponds to carboxyl stretching vibration. This band is not present in both reduced samples. The new bands in 1560.2 cm^{-1} and 1635.6 cm^{-1} [35] in the KRGO sample is indicative of carboxyl group reductions [36]. This shift confirms the decrease in oxygenated groups in carbon layers with a partial reconstruction of the carbon chain configuration.

Table 1 – Optical bandgap derivated from indirect transition extrapolation of Tauc plot.

Material	Wavelength (nm)	Bandgap (eV)
GO	233	3.67
NaRGO	270	2.64
KRGO	273	2.48

Finally, the broadband between 3000 cm^{-1} up to 3600 cm^{-1} in all samples can be observed from the attached hydroxyl on the edge of carbon layers. Despite the decrease in carboxyl and epoxy groups in reduced samples, the remains of hydroxyl can be explained by the absorption of water [37] and the attachment of glucose-derivated compounds, as discussed above.

3.2.3. *Thermogravimetric analysis*

The thermal stability of synthesized compounds was evaluated in the thermal gravimetric analyzer in air. The results are presented in Fig. 5. All the samples display three distinctive zones of weight loss, corroborated by the variation in the weight loss rate. The first event occurred between 40 and 100 °C and was attributed to humidity and absorbed ethanol from centrifugation process, with a characteristic peak of 7.7%/min at 68.8 °C in the KRGO sample, similar to observed by Kathuria et al. [38]. On the other hand, the NaRGO presented a lower rate at the same temperature, but with the presence of the same event.

The second thermal event zone occurred between 150.0 and 250.0 °C, with the decomposition of hydroxyl, carboxyl, and epoxy groups [39–41], with the displacement of maximum rate from 210.5 °C in GO to 193.5 °C in NaRGO and 184.9 °C in KRGO. Unlike the behavior at low temperatures, the highest weight loss rate was achieved by NaRGO with 10.7%/min.

The last degradation event occurred between 350.0 and 550.0 °C, mainly due to the breaking of C–C and C=C in graphene layers. The mass loss occurred at higher temperatures in GO than in the reduced samples, indicating better thermal stability of carbon chains in the oxidized form. Both NaRGO and KRGO presented the event in the same temperature window, with the presence of multiple loss rate peaks in NaRGO, while in KRGO displayed only a broad peak between 369.8 and 447.8 °C.

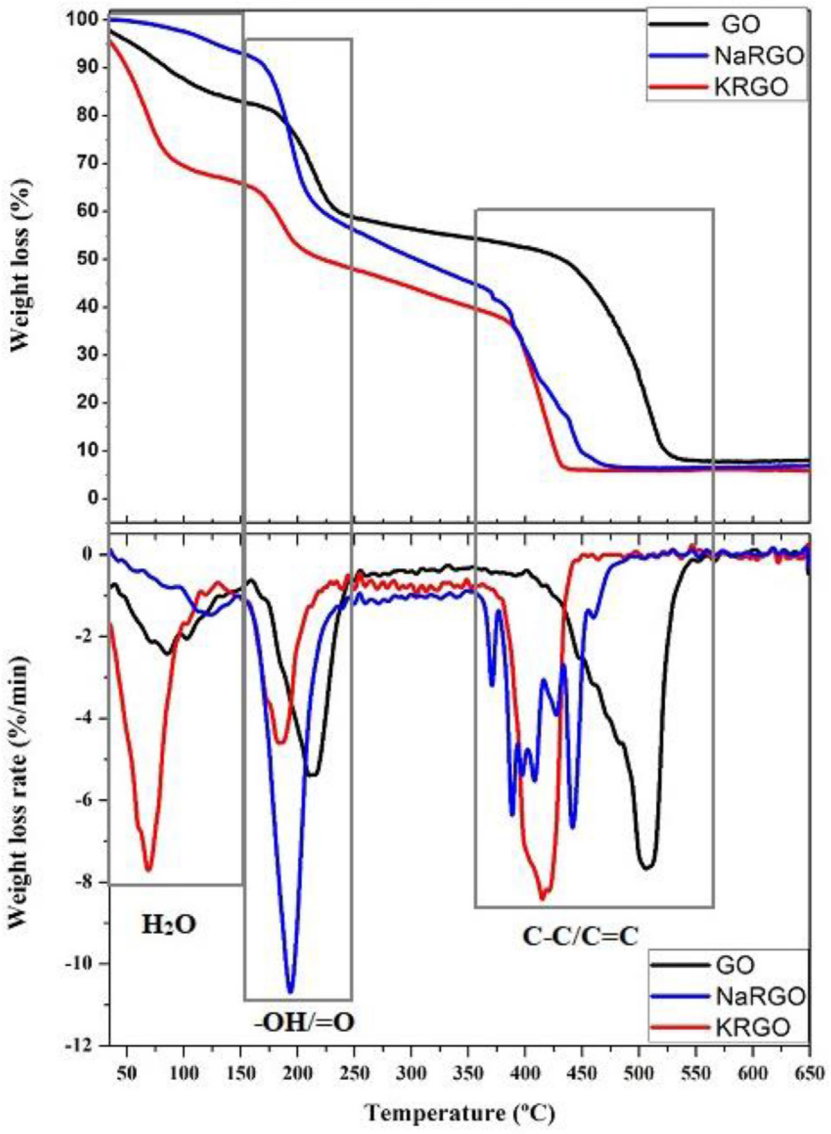

Fig. 5 – Thermogravimetric analysis of graphene derivated samples. Black line = graphene oxide, blue line as reduced graphene oxide (RGO) reduced with NaOH labeled (NaRGO), and redline as RGO reduced with KOH (KRGO).

The changes in this last event can be attributed to the variation in the density of oxygen groups and the differences between carbon lattices in GO and reduced samples, with a partial deformation on the planes due to the oxygen reduction and sonication process. The presence of glucose-derivated species attached on the material surface can be observed in Fig. S2. When the thermal analysis was recorded for GO samples after being dispersed in a glucose solution for 60 min, like in the reduced samples, the maximum loss rate reduced from 506.6 °C in GO down to 449.1 °C on glucose coated GO.

In the last event, NaRGO and KRGO exhibited differences. The samples reduced in NaOH presented several peaks, attributed to the glucose derivates presence in the sample and deformations in carbon sheets caused by sonication process, as discussed below in the diffraction results.

3.2.4. *X-ray diffraction (XRD)*

The structure modifications were evaluated with the use XRD to understand how the reduction process affects carbon layers on the graphene oxide. The results are in Fig. 6 and the obtained parameters in Table 2.

The results demonstrate the characteristic peaks attributed to the basal plane of carbon rings. The main peak in GO corresponding to (001) is at $2\theta = 10.62°$, with an interplanar distance of 0.83 nm, which is larger than exfoliated graphene sheet with 0.337 nm [1]. The intercalation of oxygen-based functional groups in carbon chain plans and on its edges causes deformation in-plane and increases (001) distance. According to Scherrer's equation, GO presents the Lc of 3.67 nm, an average width of 14.76 times the height, with 54.18 nm, and a staking of about 4.39 sheets per crystal.

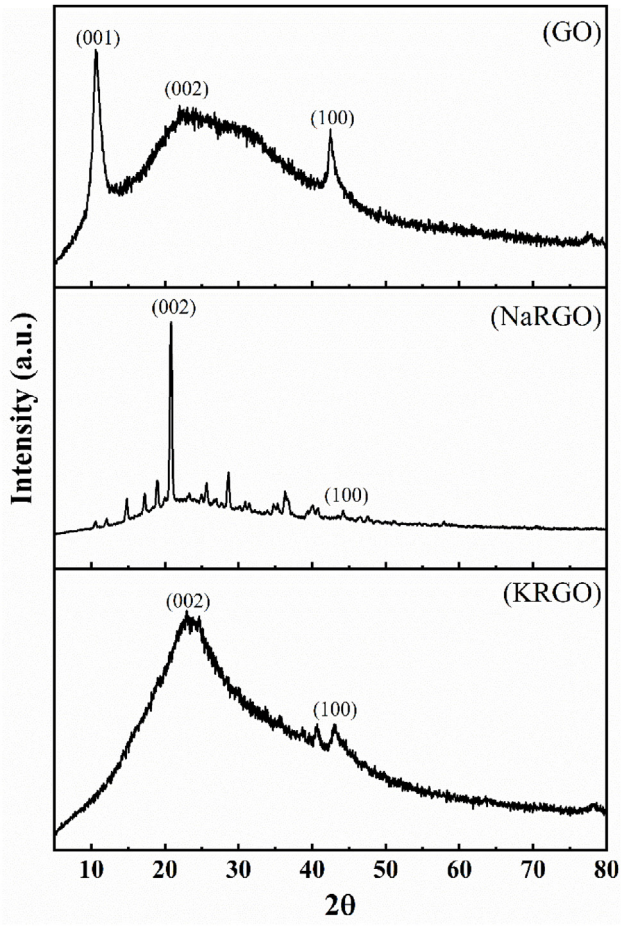

Fig. 6 – Diffraction pattern of graphene oxide, RGO reduced with NaOH labeled as NaRGO, and reduced graphene oxide reduced with KOH labeled as KRGO.

On the other hand, after the reduction process, both compounds present significant differences between them and GO, and with each other. First, they have a dislocation in the main peak, attributed to plane (002). The new reduced compounds exhibit a sharp and intense peak in $2\theta = 20.78$ for NaRGO and a broad peak in $2\theta = 23.02°$ for KRGO. In addition, only NaRGO presented several peaks attributed to the presence of residual glucose (JCPDS 024-1964), derivated to the attachment of glucose-based compounds on the RGO surface during the reduction process and increasing pH with NaOH, which can justify the sample behavior in the Thermogravimetric (TGA) analysis, with multiple peaks in weight loss rate between 350 °C and 500 °C.

The decrease in oxygen content observed in bandgap reduction and FTIR analysis are corroborated by the XRD results. The contraction of interplanar distance to 0.43 nm in NaRGO and 0.39 nm in KRGO indicates the partial restoration of carbon sp^2 sheets. The values are higher than pristine exfoliated graphene, suggesting the presence of reminiscent oxygen bonds. Another factor that contributes to the difference in interplanar distance is the possible deformation caused by the cavitation process during ultrasound-assisted reduction.

Other changes can be observed in the height and length of carbon sheets. The increase of L_c to 8.49 nm in the NaRGO sample is reflected in an increase of the carbon layers to 19.55, and the decrease in L_a to 18.65 nm, with the length, remaining 2.20 times the height. In the case of KRGO, the height reduced to 1.24 nm, with average layers reduced to 3.24, and the length reduced to 22.07, with a ratio between height and length of 17.80, the highest value of all the samples. In all reduced samples, a reduction in carbon sheet length can be observed, associated with breaks on carbon chains during the reduction of oxygen bonded to the honeycomb lattice.

3.2.5. *Microscopy characterization*

The morphology and chemical composition of all synthetized samples were analyzed using SEM and the results are presented in Fig. 7. In the GO sample, the layered stacked structure is characteristic of graphene-based materials. After the reduction process, particles maintain the wrinkle morphology in both Na and K reduced samples, which is similar to the morphology previously presented by Al-Gaashani et al. [42]. Additionally, a few layers of stacked structure can be observed in the KRGO sample, in agreement with diffraction data.

Regarding the chemical composition, the energy-dispersive X-ray spectroscopy (EDS) data presented in Fig. 7d demonstrated the presence of carbon and oxygen elements as major components, as expected in graphene oxide-based materials. Spectral data also presented manganese in all samples and sulfur in GO and KRGO, as a result of the use of potassium permanganate and sulfuric acid during the oxidation process. In the reduced products, the presence of potassium in K-based sample and sodium in the Na-based material is indicative of the incorporation of the base used in the final product.

3.2.6. *Electrochemical spectroscopy impedance (EIS)*

Some of the applications for graphene oxide-based materials are related to the electron mobility into graphene oxide and reduced graphene oxide sheet. In that context, EIS can be used to evaluate the material surface properties when applied to an external potential with response analyzed in different

Table 2 – Crystallographic parameters obtained from diffraction results.

	$2\theta_{(00)}$	$FWHM_{(001)}$	$FWHM_{(002)}$	$2\theta_{(100)}$	$FWHM_{(100)}$	D (nm)	Lc (nm)	La (nm)	N_L
GO	10.62	0.79	–	42.46	0.32	0.83	3.67	54.18	4.39
NaRGO	20.78	–	0.95	44.11	0.94	0.43	8.49	18.65	19.55
KRGO	23.02	–	6.55	42.99	0.79	0.39	1.24	22.07	3.14

2θ = angle of peaks in degrees, FWHM = Width at half the height of the corresponding diffraction peak in degree, D = distance between carbon layers, L_c = the stacking of atomic layers, L_a = carbon plane length, and N_L = average number of layers on the material unit.

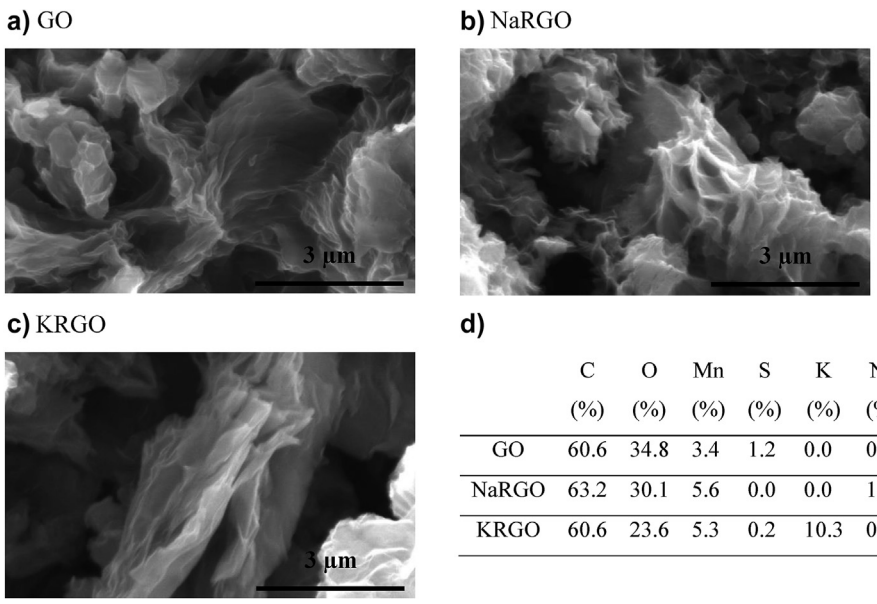

d)

	C (%)	O (%)	Mn (%)	S (%)	K (%)	Na (%)
GO	60.6	34.8	3.4	1.2	0.0	0.0
NaRGO	63.2	30.1	5.6	0.0	0.0	1.1
KRGO	60.6	23.6	5.3	0.2	10.3	0.0

Fig. 7 – Scanning electron microscopy of graphene oxide (a), RGO reduced with NaOH labeled as NaRGO (b), reduced graphene oxide reduced with KOH labeled as KRGO (c), and chemical composition of analyzed samples (d).

frequencies. In this study, the synthetized particles were coated on a platinum surface and analyzed between 1.0×10^5 and 0.1 Hz in PBS at pH 7.4. The obtained results are in Fig. 8, in the form of a Nyquist plot of the imaginary Y axis and real X axis on the graph. All samples could be fitted according to equivalent circuits, with values presented in Table 3.

The bare platinum surface presented only a simple equivalent Randles circuit, written Rs (Rct_2CPE_2), related to the resistive (Rct) and capacitive (CPE) components, with values of 1.44×10^5 Ω and 3.44×10^{-6} F, respectively. The platinum sample coated with GO presented significative changes on the Nyquist plot, indicating the effectiveness of the coating process. The fitted circuit was Rs (Rct_1CPe_1) (Rcr_2CPE_2), with an increase of two new components due to the presence of graphene oxide in the electrode surface, with values of 32.89 Ω and 25.90×10^{-4} F, corresponding to Rct_1 and CPe_1 of graphene oxide, and 2.41×10^5 Ω and 5.98×10^{-6} F, corresponding to Rct_2 and CPe_2 of the layer and Pt interface.

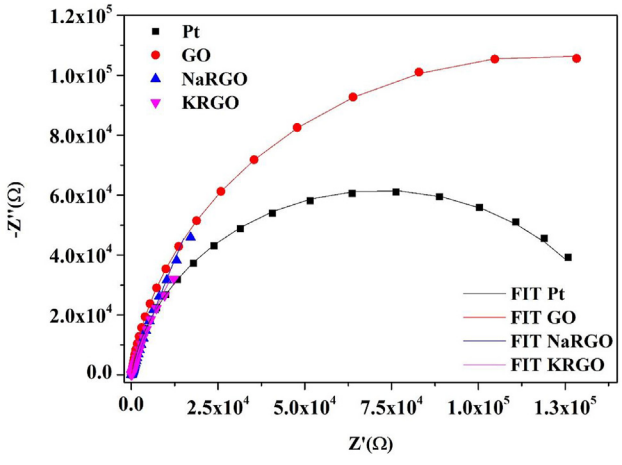

Fig. 8 – Electrochemical spectroscopy impedance results consolidated in Nyquist graph of graphene derivated samples, with bare platinum in the black line, graphene oxide as the red line, RGO reduced with NaOH labeled as NaRGO in the blue line, and reduced graphene oxide reduced with KOH labeled as KRGO in the magenta line.

Both reduced samples presented similar equivalent circuits with GO, being represented by Rs (Rct_1CPe_1) (Rcr_2CPE_2) circuit. Differing from GO, the partially reduced samples had an increase in the Rct_1 of the coating/solution interface to 105.19 Ω in NaRGO and 149.68 Ω in KRGO. On the other hand, the CPe_1 significantly decreased to 2.77 10^{-4} F and 1.83 10^{-4} F in NaRGO and KRGO, respectively.

Despite the expected reduction in the charge transfer resistance for reduced graphene [43], both partially RGOs demonstrated a significant increase in the Rct_1. This can be explained by the anchoring of glucose-derivated compounds, which can impose a barrier to the electron transference on the interface between the coating and solution [44,45]. This modification was greater in KRGO sample, possibly due to the degree of reduction associated with the presence of glucose-derivated molecules, as discussed above in the other results. Similarly, the KRGO also presented a lower value for CPe_1, associated with the accumulation of charges due to the presence of a double layer at the electrode surface.

3.2.7. *X-ray photoelectron spectroscopy (XPS)*

To understand how the reduction process affects the graphene oxide structure and its possible reaction with glucose molecules, XPS was performed using samples centrifuged in ultrapure water and dyed at 60 °C for 12 h. The obtained results are presented in Fig. 9 and Table 4.

The C1s high-resolution spectra of GO present a peak at 285.0 eV, attributed to the C–C and C=C bonds, consistent

Table 3 – Fitted data from Nyquist graph of graphene oxide (GO), reduced graphene oxide using NaOH as a base (NaRGO), and reduced graphene oxide using KOH as the base (KRGO).

	Rs (Ω)	Rct_1 (Ω)	CPE_1 (F)	Rct_2 (Ω)	CPE_2 (F)
Pt	41.13	–	–	1.44×10^5	3.44×10^{-6}
GO	35.37	32.89	25.90×10^{-4}	2.41×10^5	5.98×10^{-6}
NaRGO	34.14	105.19	$2.77\ 10^{-4}$	11.1×10^5	30.2×10^{-6}
KRGO	34.76	149.68	$1.83\ 10^{-4}$	3.46×10^5	42.9×10^{-6}

with carbon-based materials [35]. The peaks observed at 287.0 eV, 288.8 eV, and 289.6 eV are attributed to hydroxyl C–O/C–OH and/or epoxy C–O–C; carbonyl C=O; carboxyl O–C=O; respectively. Finally, the O1s high-resolution spectra have a single peak at 533.0 eV, indicating the presence of oxidized carbon material, consistent with GO [35,42].

The carbon/oxygen ratio and its respective groups are important to investigate the oxidation and reduction process of graphene-based materials, and the values are presented in Table 4. The main component of GO, Carbon is present at 73.2 at% and a C/O ratio of 2.9, with 22.58% in the area of deconvolution (A%) corresponding to C–C/C=C. In this sample, the major oxygen group corresponds to hydroxyl and/or epoxy, with 41.57 A% and a ratio of 1.841 to C–C/C=C. Second, the carbonyl represents 22.27 A%, with a ratio of 0.986 to C–C/C=C. Finally, GO has carbonyl bonds representing 13.59 A%, with a ratio of 0.602 to C–C/C=C.

After the reduction process mediated by glucose oxidation, the C1s and O1s spectra displayed significant differences from GO, with a slight decrease in carbon content (at%) in NaRGO. On the other hand, KRGO presented a notable increase, with the C/O ratio of 2.2 and 3.5. In addition, the C–C/C=C contribution area increased in both cases to 38.11 A% and 47.28 A% at 285.0 eV in NaRGO and KRGO, respectively.

This result indicates a partial reduction in GO structure, with reestablishing of ordered structure, despite the remaining oxygen groups present, which agrees with previous reports using sugars as reducing agents [20], and explains the reduction observed in the bandgap results, with major C–C/C=C in KRGO obtaining the lower bandgap value at 2.48 eV.

The hydroxyl was maintained as the major oxygen group in reduced samples, representing 41.53 A% at 286.7 eV in NaRGO and 25.20 A% at 286.3 eV in KRGO. The O/C–C also has significant differences, maintaining 1.087 and 0.533,

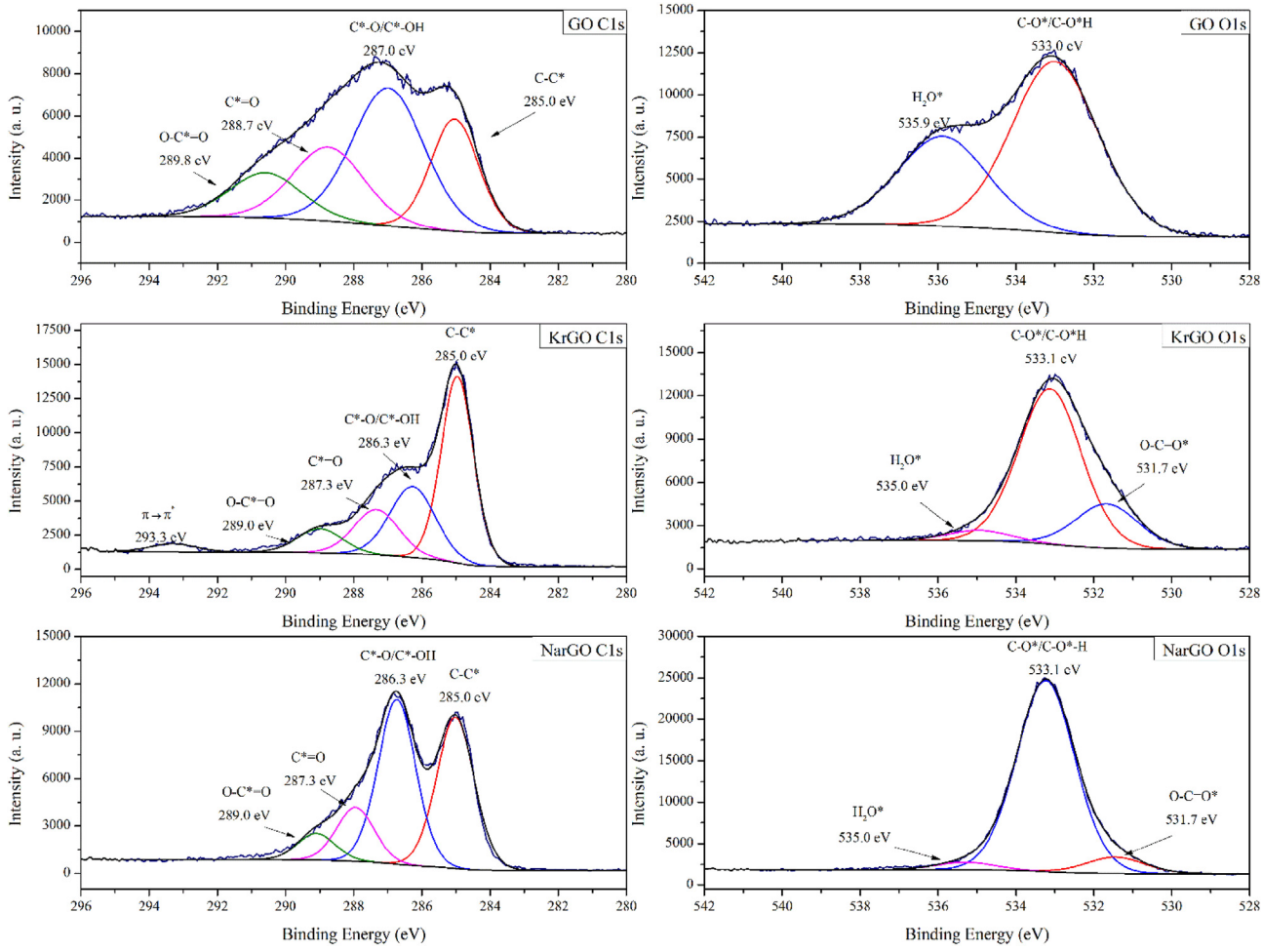

Fig. 9 – X-ray photoelectron spectroscopy spectra with C1s and O1s with their respective deconvolution for GO, KRGO, and NaRGO samples.

Table 4 – X-ray photoelectron spectroscopy results in graphene oxide (GO), reduced graphene oxide using NaOH as a base (NaRGO), and reduced graphene oxide using KOH as the base (KRGO).

	C1s				O1s			
	Position (eV)	Area (%)	Specie	O/C–C	Position (eV)	Area (%)	Specie	
GO	285.0	22.58	C*-C	–	533.0	64.94	C=O*/C–O*H	
	287.0	41.57	C*-O/C–O–C	1.841	535.9	35.06	H_2O	
	288.8	22.27	C* = O	0.986	–	–	–	
	290.6	13.59	O–C* = O	0.602	–	–	–	
	At %		Peak Area		At %	Peak Area		C/O
	73.4		1692.73		25.1	1699.41		2.9
KRGO	285.0	47.28	C*-C	–	531.7	21.00	C=O*/O–C=O*	
	286.3	25.20	C*-O	0.533	533.2	88.87	C–O*/C–O*H	
	287.3	16.05	C–O–C	0.339	535.1	3.53	H_2O	
	289.0	8.49	O–C* = O	0.180	–	–	–	
	293.3	2.99	π-π* Satellite/K2$p_{3/2}$		–	–	–	
	At %		Peak Area		At %	Peak Area		C/O
	77.8		1357.62		22.2	1136.13		3.5
NaRGO	285.0	38.11	C*-C	–	531.5	7.60	C=O*/O–C=O*	
	286.7	41.53	C*-O	1.087	533.2	88.87	C–O*/C–O*H	
	288.0	13.62	C* = O/C–O–C	0.357	535.3	1.15	H_2O	
	289.1	6.74	O–C=O	0.177				
	At %		Peak Area		At %	Peak Area		C/O
	68.4		1468.25		31.1	1953.46		2.2

& The GO sample has the presence of 1.5 At% of S.
# The NaRGO sample has the presence of 0.5 At% of Na.

indicating that NaRGO has twice the hydroxyl content as KRGO in relation to C–C/C=C. This could indicate the preference for the attack of hydroxyl with the use of KOH as the base for reduction.

Another difference is observed in the other reminiscent groups. The presence of 13.62 A% of carbonyl/epoxy at 288.0 eV in NaRGO represents a ratio of 0.357 in relationship to C–C/C=C. On the other hand, KRGO has a remaining epoxy in 16.05 A% at 287.3 eV, with a ratio of 0.339 in relationship to C–C/C=C. The presence of epoxy bonding can be assigned to the chemical interaction of GO and gluconic acid during the reduction process [15]. The possible overlap of π-π* Satellite and K2$p_{3/2}$ signal at 293.3 eV is also observed only on KRGO, representing 2.99 A%. Similarly, the possible presence of Na in NaRGO represents 0.5 At% in the sample.

Another indication of the gluconic acid attachment is observed in both reduced samples, consisting of the presence of 6.74 A% and 8.49 A% of carboxyl at 289.1 eV and 289.0 eV in NaRGO and KRGO, respectively. The similar O/C–C ratios, representing 0.177 and 0.180 can also be attributed to the difference in hydroxyl content between samples reduced with NaOH and KOK with the partial reduction. However, the attachment of glucose-derivated compounds in the material surface indicates a greater attachment in NaRGO, which agrees with the presence of derivated glucose observed on XRD peaks and several thermogravimetric events between 350 and 550 °C.

The O1s spectra in Fig. 9 also exhibits differences between GO and the reduced samples. The oxygen content represents 25.1 At% in the GO sample, with an increase to 31.1 At% in NaRGO, and a decrease to 2.2At% in KRGO. This difference can be associated not only with the reduction degree but also with the preferred attachment of the gluconic acid on Na reduced sample, which can be corroborated by the increase of C–C/C=C bond on the reduced sample with Na. This indicates the partial restoration of graphene oxide and its effective reduction [20], with a consequence attachment of gluconic acid at the particle surface.

Regarding the presence of different groups in the samples, the GO presents two peaks in 533.0 eV associated with hydroxyl and carbonyl bonds representing 64.94 A%, with a slight displacement to 533.2 eV and 533.1 eV in NaRGO and KRGO, representing 7.6 A% and 21.0 A%, respectively. Another peak at 535.9 eV in GO is associated with adsorbed water, representing 35.06 A%, and is at 535.3 eV (3.53 A%) and 535.0 eV (3.85 A%) in NaRGO and KRGO, respectively.

In the reduced samples, an additional peak is observed at 531.5 eV in NaRGO and 531.7 eV in KRGO, which was associated with the double bonded C=O in carbonyl and carboxyl, representing 7.6 A% and 21.0 A%, respectively. This could be due to the presence of reminiscent carbonyl on graphene sheets and is also associated with the presence of glucose-derivated compounds, as gluconic acid linked to hydroxyl bond in RGO [15,20]agrees with the obtained TGA and XRD results and can explain the good stability of RGO solutions, which disagree with previous reports about RGO solubility in water [37,46].

4. Conclusions

This work investigated the influence of the base on the reduction process assisted by probe sonication in the presence of glucose as a reducing agent. The use of glucose-based

reduction provides the attachment of glucose-oxidized molecules at reduced graphene oxide, acting as a capping agent, and stabilizing the particles in the aqueous solution for further applications.

Despite the information presented in previous publications, this article demonstrated the relationship between the chosen base and reduced product. The different reminiscent oxygen groups promoted were confirmed by differences in the bandgap between 3.67 eV and 2.48 eV in the reduced form with KOH, with an interplanar distance of 0.39 nm, which is a little higher than pristine graphene.

Regarding the electron transfer ability in the proposed partially reduced samples, the sodium-based material also presented lower resistivity than KRGO, with a value of 105.19 Ω to NaRGO and 149.68 Ω to KRGO, indicating the influence of base in the impedance properties of the partially reduced samples.

Additionally, the observed results indicate different percentages of oxygen groups in the material and a preference for gluconic acid attachment of NaRGO, in contrast with the KRGO sample, confirmed in thermogravimetric profile and X-ray photoelectron O/C–C rates. Thus, this study evidences new ways to determine the adequate glucose-based reduction route, according to desired properties and application, such as UV–Vis absorption and bandgap regulation to catalysis and electrocatalysis, C/O rate for biological applications, and molecules chelation thermal stability for high-temperature applications.

Funding

This study was financed in part by the Coordenação de Aperfeiçoamento de Pessoal de Nível Superior - Brasil (CAPES) - Finance Code 001 and the Fundação de Amparo à Pesquisa do Estado do Amazonas (FAPEAM). This research was partially funded by the Fundação de Amparo a Pesquisa do Estado de São Paulo (FAPESP) by the Centro de Desenvolvimento de Materias Funcionais (CDMF) Grant 2013/07296-2.

CRediT authorship contribution statement

Jean Valdir Uchôa Teixeira: Conceptualization, Methodology, Writing – original draft. **Gabriel Junior Cavalcante Pimentel:** Investigation, Formal analysis, Writing – original draft. **Adriana Alencar Santos:** Methodology, Writing – original draft. **Leonardo Francisco Gonçalves Dias:** Methodology, Investigation, Formal analysis, Writing – review & editing. **Valmor Roberto Mastelaro:** XPS measurements, data analysis, and Writing. **Paulo Noronha Lisboa Filho:** Conceptualization, Supervision, Writing – review & editing, Resources.

Data availability

The datasets generated during and/or analyzed during the current study are available from the corresponding author upon reasonable request.

Declaration of Competing Interest

The authors declare no conflicts of interest.

Acknowledgments

The authors acknowledge Prof. Gilbert Bannach for the TGA measurements. The authors acknowledge The Instituto de Estudos Avançados do Mar (IEMAR) for allowing to use the electrochemical equipment. The authors acknowledge the following funders by financial support: Coordenação de Aperfeiçoamento de Pessoal de Nível Superior - Brasil (CAPES) - Finance Code 001, Fundação de Amparo à Pesquisa do Estado de São Paulo (FAPESP) by the Centro de Desenvolvimento de Materiais Funcionais (CDMF) Grant 2013/07296-2 and Fundação de Amparo à Pesquisa do Estado do Amazonas (FAPEAM) - Finance Code N001/2019-PROPG-CAPES/FAPEAM.

Appendix A. Supplementary data

Supplementary data to this article can be found online at https://doi.org/10.1016/j.jmrt.2023.07.211.

REFERENCES

[1] Kumar N, Srivastava VC. Simple synthesis of large graphene oxide sheets via electrochemical method coupled with oxidation process. ACS Omega 2018;3:10233–42. https://doi.org/10.1021/acsomega.8b01283.

[2] Liu W, Speranza G. Tuning the oxygen content of reduced graphene oxide and effects on its properties. ACS Omega 2021;6:6195–205. https://doi.org/10.1021/acsomega.0c05578.

[3] Zhou Q, Xia G, Du M, Lu Y, Xu H. Scotch-tape-like exfoliation effect of graphene quantum dots for efficient preparation of graphene nanosheets in water. Appl Surf Sci 2019;483:52–9. https://doi.org/10.1016/j.apsusc.2019.03.290.

[4] Lemine AS, Zagho MM, Altahtamouni TM, Bensalah N. Graphene a promising electrode material for supercapacitors—a review. Int J Energy Res 2018;42:4284–300. https://doi.org/10.1002/er.4170.

[5] Zhu Y, Kong G, Pan Y, Liu L, Yang B, Zhang S, et al. An improved Hummers method to synthesize graphene oxide using much less concentrated sulfuric acid. Chin Chem Lett 2022. https://doi.org/10.1016/j.cclet.2022.01.060.

[6] Olorunkosebi AA, Eleruja MA, Adedeji AV, Olofinjana B, Fasakin O, Omotoso E, et al. Optimization of graphene oxide through various Hummers' methods and comparative reduction using green approach. Diam Relat Mater 2021;117. https://doi.org/10.1016/j.diamond.2021.108456.

[7] Zhu C, Guo S, Fang Y, Dong S. Reducing sugar: new functional molecules for the green synthesis of graphene nanosheets. ACS Nano 2010;4:2429–37. https://doi.org/10.1021/nn1002387.

[8] Agarwal V, Zetterlund PB. Strategies for reduction of graphene oxide – a comprehensive review. Chem Eng J 2021;405. https://doi.org/10.1016/j.cej.2020.127018.

[9] Thakur S, Karak N. Alternative methods and nature-based reagents for the reduction of graphene oxide: a review. Carbon N Y 2015;94:224–42. https://doi.org/10.1016/j.carbon.2015.06.030.

[10] de Silva KKH, Huang HH, Joshi RK, Yoshimura M. Chemical reduction of graphene oxide using green reductants. Carbon N Y 2017;119:190–9. https://doi.org/10.1016/j.carbon.2017.04.025.
[11] Aunkor MTH, Mahbubul IM, Saidur R, Metselaar HSC. The green reduction of graphene oxide. RSC Adv 2016;6:27807–25. https://doi.org/10.1039/c6ra03189g.
[12] Muthoosamy K, Geetha Bai R, Abubakar IB, Sudheer SM, Lim HN, Loh HS, et al. Exceedingly biocompatible and thin-layered reduced graphene oxide nanosheets using an eco-friendly mushroom extract strategy. Int J Nanomed 2015;10:1505–19. https://doi.org/10.2147/IJN.S75213.
[13] He D, Shen L, Zhang X, Wang Y, Bao N, Kung HH. An efficient and eco-friendly solution-chemical route for preparation of ultrastable reduced graphene oxide suspensions. AIChE J 2014;60:2757–64. https://doi.org/10.1002/aic.14499.
[14] Arias FA, Guevara M, Tene T, Angamarca P, Molina R, Valarezo A, et al. The adsorption of methylene blue on eco-friendly reduced graphene oxide. Nanomaterials 2020;10. https://doi.org/10.3390/nano10040681.
[15] Akhavan O, Ghaderi E, Aghayee S, Fereydooni Y, Talebi A. The use of a glucose-reduced graphene oxide suspension for photothermal cancer therapy. J Mater Chem 2012;22:13773–81. https://doi.org/10.1039/c2jm31396k.
[16] Alemi F, Zarezadeh R, Sadigh AR, Hamishehkar H, Rahimi M, Majidinia M, et al. Graphene oxide and reduced graphene oxide: efficient cargo platforms for cancer theranostics. J Drug Deliv Sci Technol 2020;60. https://doi.org/10.1016/j.jddst.2020.101974.
[17] Lima-Sousa R, de Melo-Diogo D, Alves CG, Costa EC, Ferreira P, Louro RO, et al. Hyaluronic acid functionalized green reduced graphene oxide for targeted cancer photothermal therapy. Carbohydr Polym 2018;200:93–9. https://doi.org/10.1016/j.carbpol.2018.07.066.
[18] Hu Y, He L, Ding J, Sun D, Chen L, Chen X. One-pot synthesis of dextran decorated reduced graphene oxide nanoparticles for targeted photo-chemotherapy. Carbohydr Polym 2016;144:223–9. https://doi.org/10.1016/j.carbpol.2016.02.062.
[19] Mukherjee A, Chakrabarty S, Su WN, Basu S. Nanostructured nickel ferrite embedded in reduced graphene oxide for electrocatalytic hydrogen evolution reaction. Mater Today Energy 2018;8:118–24. https://doi.org/10.1016/j.mtener.2018.03.004.
[20] Xu C, Shi X, Ji A, Shi L, Zhou C, Cui Y. Fabrication and characteristics of reduced graphene oxide produced with different green reductants. PLoS One 2015;10. https://doi.org/10.1371/journal.pone.0144842.
[21] Stempien Z, Khalid M, Kozicki M, Kozanecki M, Varela H, Filipczak P, et al. In-situ deposition of reduced graphene oxide layers on textile surfaces by the reactive inkjet printing technique and their use in supercapacitor applications. Synth Met 2019;256. https://doi.org/10.1016/j.synthmet.2019.116144.
[22] Ji A, Chen Y, Wang X, Xu C. Inkjet printed flexible electronics on paper substrate with reduced graphene oxide/carbon black ink. J Mater Sci Mater Electron 2018;29:13032–42. https://doi.org/10.1007/s10854-018-9425-1.
[23] Sharma K, Maiti K, Kim NH, Hui D, Lee JH. Green synthesis of glucose-reduced graphene oxide supported Ag-Cu2O nanocomposites for the enhanced visible-light photocatalytic activity. Compos B Eng 2018;138:35–44. https://doi.org/10.1016/j.compositesb.2017.11.021.
[24] Praxedes FM, Moreno H, Simões AZ, Teixeira VC, Nunes RS, Amoresi RAC, et al. Interface matters: design of an efficient CaCu3Ti4O12-rGO photocatalyst. Powder Technol 2022:117478. https://doi.org/10.1016/j.powtec.2022.117478.
[25] Velasco-Soto MA, Pérez-García SA, Alvarez-Quintana J, Cao Y, Nyborg L, Licea-Jiménez L. Selective band gap manipulation of graphene oxide by its reduction with mild reagents. Carbon N Y 2015;93:967–73. https://doi.org/10.1016/j.carbon.2015.06.013.
[26] Pei S, Cheng HM. The reduction of graphene oxide. Carbon N Y 2012;50:3210–28. https://doi.org/10.1016/j.carbon.2011.11.010.
[27] Yasui K. Production of O Radicals from cavitation bubbles under ultrasound. Molecules 2022;27. https://doi.org/10.3390/molecules27154788.
[28] Peng K, Qin FGF, Jiang R, Qu W, Wang Q. Production and dispersion of free radicals from transient cavitation Bubbles: an integrated numerical scheme and applications. Ultrason Sonochem 2022;88. https://doi.org/10.1016/j.ultsonch.2022.106067.
[29] Aliyev E, Filiz V, Khan MM, Lee YJ, Abetz C, Abetz V. Structural characterization of graphene oxide: surface functional groups and fractionated oxidative debris. Nanomaterials 2019;9. https://doi.org/10.3390/nano9081180.
[30] Ismail Z. Green reduction of graphene oxide by plant extracts: a short review. Ceram Int 2019;45:23857–68. https://doi.org/10.1016/j.ceramint.2019.08.114.
[31] Yang G, Li L, Lee WB, Ng MC. Structure of graphene and its disorders: a review. Sci Technol Adv Mater 2018;19:613–48. https://doi.org/10.1080/14686996.2018.1494493.
[32] Nandanapalli KR, Mudusu D, Lee S. Functionalization of graphene layers and advancements in device applications. Carbon N Y 2019;152:954–85. https://doi.org/10.1016/j.carbon.2019.06.081.
[33] Kuila A, Maity N, Layek RK, Nandi AK. On the pH sensitive optoelectronic properties of amphiphilic reduced graphene oxide via grafting of poly(dimethylaminoethyl methacrylate): a signature of p- and n-type doping. J Mater Chem A Mater 2014;2:16039–50. https://doi.org/10.1039/c4ta03408b.
[34] Omidvar A, Rashidianvaziri MR, Jaleh B, Partovi Shabestari N, Noroozi M. Metal-enhanced fluorescence of graphene oxide by palladium nanoparticles in the blue-green part of the spectrum. Chin Phys B 2016;25. https://doi.org/10.1088/1674-1056/25/11/118102.
[35] Ossonon BD, Bélanger D. Synthesis and characterization of sulfophenyl-functionalized reduced graphene oxide sheets. RSC Adv 2017;7:27224–34. https://doi.org/10.1039/c6ra28311j.
[36] Lu J, Li Y, Li S, Jiang SP. Self-assembled platinum nanoparticles on sulfonic acid-grafted graphene as effective electrocatalysts for methanol oxidation in direct methanol fuel cells. Sci Rep 2016;6. https://doi.org/10.1038/srep21530.
[37] Ma J, Liu J, Zhu W, Qin W. Solubility study on the surfactants functionalized reduced graphene oxide. Colloids Surf A Physicochem Eng Asp 2018;538:79–85. https://doi.org/10.1016/j.colsurfa.2017.10.071.
[38] Kathuria A, Pauwels AK, Buntinx M, Shin J, Harding T. Inclusion of ethanol in a nano-porous, bio-based metal organic framework. J Inclusion Phenom Macrocycl Chem 2019;95:91–8. https://doi.org/10.1007/s10847-019-00920-y.
[39] Chu HJ, Lee CY, Tai NH. Green reduction of graphene oxide by Hibiscus sabdariffa L. to fabricate flexible graphene electrode. Carbon N Y 2014;80:725–33. https://doi.org/10.1016/j.carbon.2014.09.019.
[40] Some S, Kim Y, Yoon Y, Yoo H, Lee S, Park Y, et al. High-quality reduced graphene oxide by a dual-function chemical reduction and healing process. Sci Rep 2013;3. https://doi.org/10.1038/srep01929.
[41] Farivar F, Lay Yap P, Karunagaran RU, Losic D. Thermogravimetric analysis (TGA) of graphene materials: effect of particle size of graphene, graphene oxide and graphite on thermal parameters. C (Basel). 2021;7:41. https://doi.org/10.3390/c7020041.

[42] Al-Gaashani R, Najjar A, Zakaria Y, Mansour S, Atieh MA. XPS and structural studies of high quality graphene oxide and reduced graphene oxide prepared by different chemical oxidation methods. Ceram Int 2019;45:14439–48. https://doi.org/10.1016/j.ceramint.2019.04.165.

[43] Bonanni A, Pumera M. High-resolution impedance spectroscopy for graphene characterization. Electrochem Commun 2013;26:52–4. https://doi.org/10.1016/j.elecom.2012.10.013.

[44] Huang Y, Hara A, Terashima C, Fujishima A, Takai M. Protein adsorption behavior on reduced graphene oxide and boron-doped diamond investigated by electrochemical impedance spectroscopy. Carbon N Y 2019;152:354–62. https://doi.org/10.1016/j.carbon.2019.06.023.

[45] Li S, Zhang Q, Lu Y, Ji D, Zhang D, Wu J, et al. One step electrochemical deposition and reduction of graphene oxide on screen printed electrodes for impedance detection of glucose. Sensor Actuator B Chem 2017;244:290–8. https://doi.org/10.1016/j.snb.2016.12.142.

[46] Konios D, Stylianakis MM, Stratakis E, Kymakis E. Dispersion behaviour of graphene oxide and reduced graphene oxide. J Colloid Interface Sci 2014;430:108–12. https://doi.org/10.1016/j.jcis.2014.05.033.